Journal of Alloys and Compounds 574 (2013) 240–245

Contents lists available at SciVerse ScienceDirect

Journal of Alloys and Compounds

journal homepage: www.elsevier.com/locate/jalcom

Controllable photoluminescent–magnetic dual-encoded wurtzite ZnS:$Cu^{2+}Mn^{2+}$ nanowires modulated by Cu^{2+} and Mn^{2+} ions

Jinghai Yang [a,b,c,*], Bingji Wang [a,b], Jian Cao [a,b,*], Donglai Han [a,b,c], Bo Feng [a,b,c], Maobin Wei [a,b], Lin Fan [a,b], Chunlei Kou [d], Qianyu Liu [a,b], Tingting Wang [a,b]

[a] The Institute of Condensed State Physics, Jilin Normal University, Siping 136000, PR China
[b] Key Laboratory of Functional Materials Physics and Chemistry of the Ministry of Education, Jilin Normal University, Siping 136000, PR China
[c] Key Laboratory of Excited State Physics, Changchun Institute of Optics, Fine Mechanics and Physics, Chinese Academy of Sciences, 3888 Eastern Nan-Hu Road, Changchun 130033, PR China
[d] College of Physics, Beihua University, Jilin 132013, PR China

ARTICLE INFO

Article history:
Received 27 November 2012
Received in revised form 2 May 2013
Accepted 2 May 2013
Available online 9 May 2013

Keywords:
Hydrothermal
ZnS:$Cu^{2+}Mn^{2+}$
Photoluminescence
Ferromagnetism

ABSTRACT

The wurtzite-type ZnS:$Cu^{2+}Mn^{2+}$ nanowires (NWs) were prepared by a simple hydrothermal method at 180 °C without any surface-active agent. The results of XRD, EDAX and XPS showed that both the Cu^{2+} and Mn^{2+} ions were incorporated into the ZnS lattice. The maximum concentration of the Cu^{2+} ions in the ZnS and $Zn_{0.99}Mn_{0.01}S$ NWs was 7% and 1%, respectively. The maximum concentration of the Mn^{2+} ions in the $Zn_{0.99}Cu_{0.01}S$ NWs can reach to 10%. The ZnS:Cu^{2+} NWs exhibited the Cu^{2+}-related emission peak centered at 540 nm coming from sulfur vacancy to t^2 level of Cu^{2+}, while the ZnS:$Cu^{2+}Mn^{2+}$ NWs exhibited the Mn^{2+} ($^4T_1-^6A_1$) and Cu^{2+} (interstitial S to t^2 level of Cu^{2+}) related transition centered at 577 nm and 501 nm, respectively. Moreover, the ZnS:$Cu^{2+}Mn^{2+}$ NWs showed the room temperature ferromagnetism property, and the saturation magnetization was increased as the Mn^{2+} doped ratio increased.

1. Introduction

With the rapidly advanced research of the II–VI semiconductor nanomaterials [1–5], the transition metal ions doped ZnS nanocrystals with tunable and stable emission in visible as well as in near-IR spectral region [6–8] exhibit a great application prospect in the field of the biology science [9–12]. The doping ions can create the intermediate energy state between the valence band and conduction band of the ZnS and change its photophysical relaxation process. Usually, Mn and Cu doped ZnS nanocrystals are demonstrated as the efficient phosphor because of the blue to orange light emission [13–16]. For Mn doped ZnS nanocrystals, the emission is restricted within the yellow–orange region (580–600 nm) coming from the Mn^{2+} $^4T_1-^6A_1$ transition [17–20]. For Cu doped ZnS nanocrystals, a wide range of the blue–green emission through the recombination of the electron in the conduction band or defects of the ZnS and the hole in Cu t^2 state can be obtained [14,21,22]. Therefore, Mn/Cu co-doped ZnS nanocrystals could be a potentially color tunable phosphor to serve as a new class of white light-emitting materials [23,24]. Based on the literature [25], the photorelaxation process of the dual-doped nanocrystals can switch from one dopant to another and back again to its original state by tuning the band-gap of the nanocrystals. It is worth to note that the Cu-doped ZnS nanocrystals are not investigated as widely as the Mn-doped ZnS nanocrystals since that the Cu^{2+} ions cannot incorporate into the ZnS lattice easily like the Mn^{2+} ions and the uniform model of the optical transition process after Cu^{2+} doping has not been established. In the past few years, most studies were reported for the cubic ZnS:Cu^{2+} nanoparticles [26–30], however, little work was reported for the wurtzite ZnS:Cu^{2+} nanowires (NWs). Exploring the highly crystalline wurtzite ZnS:Cu^{2+} NWs has always been a hot and challenging topic owing to its excellent optical properties. Moreover, many researchers have confirmed that the Mn/Cr doped ZnS [31], Mn/Fe doped ZnS [32] and Cu/Cr doped ZnS [33] showed the room temperature ferromagnetism in the experiments. Since that doping two different ions into the ZnS lattice can adjust the magnetic properties, such as the mobility, the type and the concentration of charge carriers. Consequently, we were stimulated in studying if we can obtain the room temperature ferromagnetism in Mn/Cu co-doped ZnS NWs.

In this paper, we investigate systematically the optical properties of the wurtzite ZnS:$Cu^{2+}Mn^{2+}$ NWs by fixing the concentration of the Mn^{2+} ions and varying the concentration of the Cu^{2+} ions and vice versa. It would be useful to identify the maximum

* Corresponding authors. Address: The Institute of Condensed State Physics, Jilin Normal University, Siping 136000, PR China. Tel.: +86 434 3290009; fax: +86 434 3294566.
E-mail addresses: jhyang1@jlnu.edu.cn (J. Yang), caojian_928@163.com (J. Cao).

0925-8388/$ - see front matter © 2013 Elsevier B.V. All rights reserved.
http://dx.doi.org/10.1016/j.jallcom.2013.05.004

and optimum doping concentration of the Cu^{2+} ions in the ZnS and $Zn_{0.99}Mn_{0.01}S$ NWs, and the Mn^{2+} ions in the $Zn_{0.99}Cu_{0.01}S$ NWs. More importantly, we observe the room temperature ferromagnetism of the Mn/Cu co-doped ZnS NWs in the experiment, and investigate the effect of the concentration of the Mn^{2+} ions on its ferromagnetic properties.

2. Experimental section

2.1. Preparation

In our experiments, all chemicals were analytical grade and were used as received without further purification. The ZnS:$Cu^{2+}Mn^{2+}$ NWs were synthesized by the hydrothermal method, similar to our previous work [34]. Firstly, zinc nitrate, manganese nitrate and copper nitrate with appropriate proportions were dissolved in 16 ml ethylenediamine (EN) and water (1:1 in volume ratio). After stirring for 1 h, thiourea (3 mmol) was put into the resulting solution. After stirring for another 2 h, the colloid solution was transferred into a 20 ml Teflon-lined autoclave and kept at 180 °C for 12 h. After the reaction, the autoclave was taken out and cooled down to the room temperature. The product was washed with ethanol and deionized water for several times and separated by centrifugation, then dried at 80 °C for 1 h to get a white powder.

2.2. Characterization

X-ray diffraction (XRD) pattern was collected on a MAC Science MXP-18 X-ray diffractometer using a Cu target radiation source. Transmission electron micrographs (TEM) and high-resolution transmission electron microscopy (HRTEM) images were taken on JEM-2100 electron microscope. The specimen was prepared by depositing a drop of the dilute solution of the sample in ethanol on a carbon-coated copper grid and drying at room temperature. X-ray photoelectron spectrum (XPS) measurement was performed on a Vgescalab MK II X-ray photoelectron spectrometer (XPS) using Mg Kα radiation ($h\nu$ = 1253.6 eV) with a resolution of 1.0 eV. UV–vis absorption spectrum was measured on UV-3101PC UV spectrometer. The specimen was dispersed in ethanol and placed in a 1 cm quartz cell, and ethanol served as the reference. Photoluminescence (PL) measurement was carried out at room temperature, using 325 nm as the excitation wavelength, He–Cd Laser as the source of excitation. Magnetic hysteresis loop was measured by a Lake Shore 7407 vibrating sample magnetometer (VSM) with the maximum field of 6 kOe.

3. Results and discussion

Fig. 1 shows the XRD patterns of the ZnS:Cu^{2+} (x%) (x = 0, 1, 3, 5, 7, 10, 11, 12), $Zn_{0.99}Mn_{0.01}S:Cu^{2+}$($y$%) ($y$ = 1, 2, 3, 5, 7, 10) and $Zn_{0.99}Cu_{0.01}S:Mn^{2+}$ (z%) (z = 1, 5, 10) NWs. It can be seen that all the diffraction peaks of the ZnS NWs (Fig. 1a) can be well indexed as the hexagonal wurtzite structure, which are consistent with the standard card (JCPDS No. 36-1450). It is possible to predict the growth direction by performing comparison of the full width at half maximum (FWHM) for different XRD peaks. Note that the (002) diffraction peak is stronger and narrower than the other peaks, suggesting a preferential growth direction along the c-axis. The Cu^{2+} ions (0.71 nm) and Zn^{2+} ions (0.74 nm) have very similar ionic radii, so the position of the diffraction peak has no apparent change in Fig. 1a and b. For the $Zn_{0.99}Cu_{0.01}S:Mn^{2+}$ (z%) (z = 1, 5, 10) NWs, the position of the diffraction peak shifts to the low angle (Fig. 1c), indicating that the lattice constants of the $Zn_{0.99}Cu_{0.01}S:Mn^{2+}$ (z%) NWs are increased as the Mn^{2+} doped ratio increased. According to the Bragg equation [35], a slight increase of the lattice constant "a" and "c" are obtained (Fig. 1d), because the ionic radius of the Mn^{2+} ions (0.83 nm) is about 10% larger than that of the Zn^{2+} ions (0.74 nm) [36]. After incorporating the Cu^{2+} ions into the ZnS and $Zn_{0.99}Mn_{0.01}S$ lattice, the peak centered at 32.281° and 46.321° can be indexed as the Cu_2S phase (JCPDS No. 02-1284), which firstly emerged for the ZnS:Cu^{2+}(10%) and $Zn_{0.99}Mn_{0.01}S:Cu^{2+}$(2%) NWs. So the substitution ability of the Cu^{2+} ions in the $Zn_{0.99}Mn_{0.01}S$ NWs is lower than that in the ZnS NWs. In other words, the Mn^{2+}

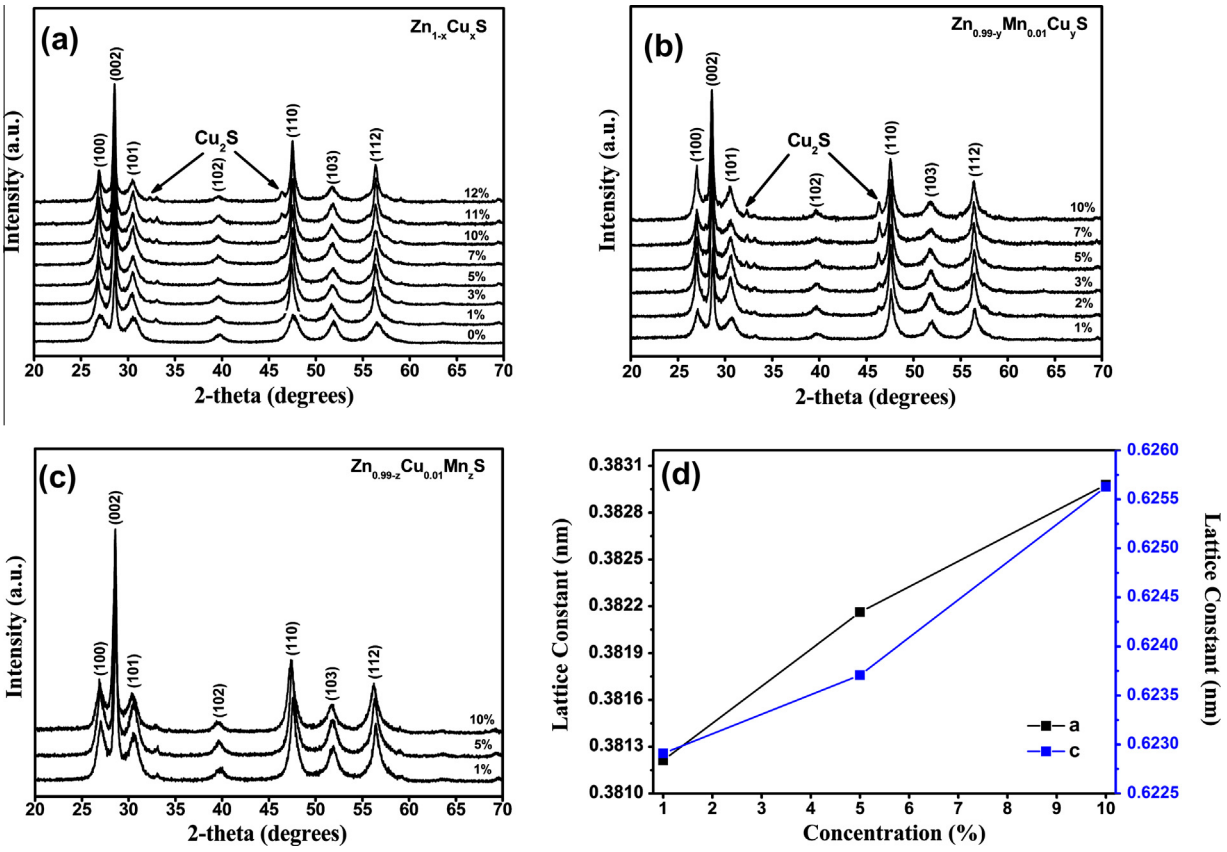

Fig. 1. XRD patterns of (a) ZnS:Cu^{2+}(x%) (x = 0, 1, 3, 5, 7, 10, 11, 12) NWs; (b) ZnS:Mn^{2+}(1%)Cu^{2+}(y%) (y = 1, 2, 3, 5, 7, 10) NWs; (c) ZnS:Cu^{2+}(1%)Mn^{2+}(z%) (z = 1, 5, 10) NWs; (d) the lattice constants of the ZnS:Cu^{2+}(1%)Mn^{2+}(z%) (z = 1, 5, 10) NWs.

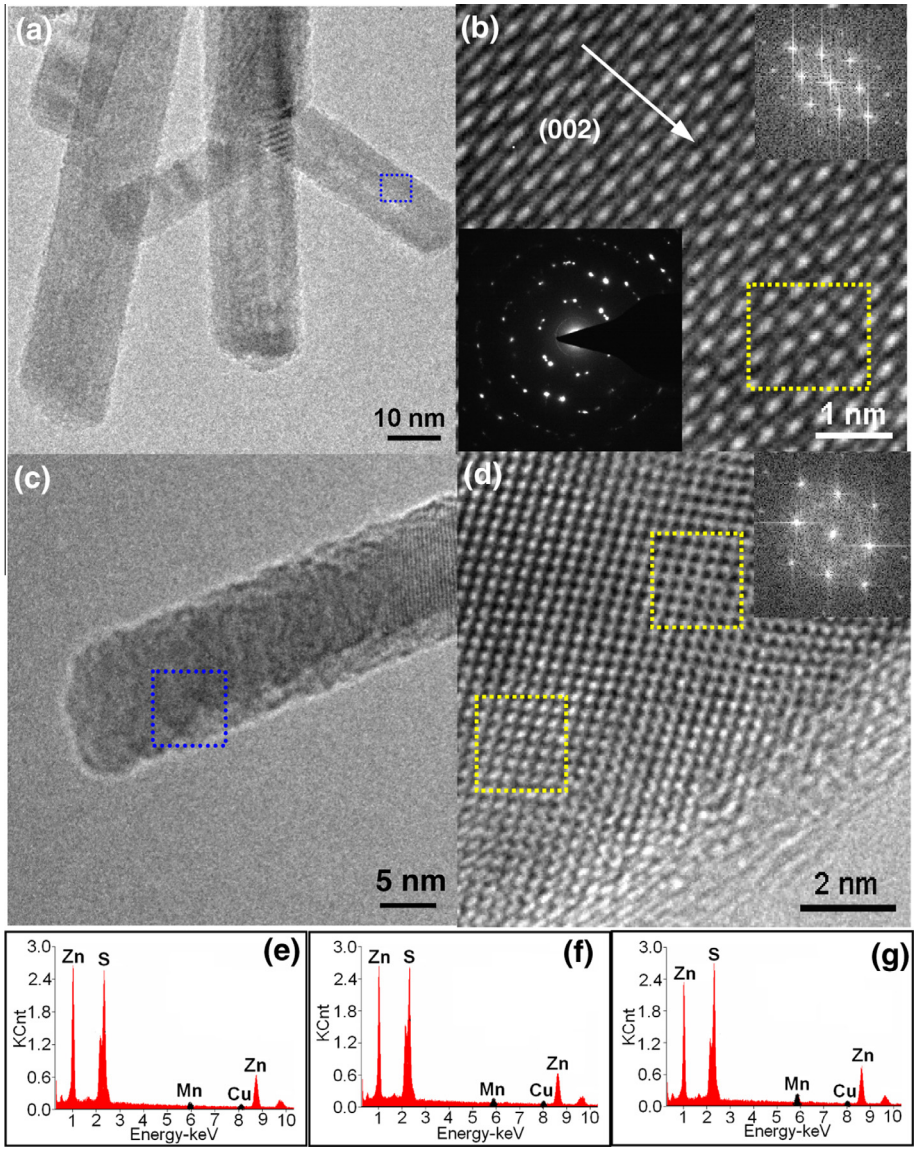

Fig. 2. (a and b) TEM and HRTEM (FFT, SAED) images of the ZnS:Cu^{2+}(1%) NWs; (c and d) TEM and HRTEM (FFT) images of the ZnS:Cu^{2+}(1%)Mn^{2+}(5%) NWs; (e–g) EDAX images of the ZnS:Cu^{2+}(1%)Mn^{2+}(1%), ZnS:Cu^{2+}(1%)Mn^{2+}(5%) and ZnS:Cu^{2+}(1%)Mn^{2+}(10%) NWs.

ions can promote the transition from the Cu^{2+} ions to the Cu^{+} ions. It is worth to note that there are no other diffraction peaks from Mn^{2+} and Cu^{2+} ions when inverse adding Mn^{2+} ions into the ZnS:Cu^{2+} (1%) NWs until the content of the Mn^{2+} ions reach to 10% (Fig. 1c). The Cu^{2+} ions cannot be doped into the ZnS lattice easily due to the less solubility of CuS in ZnS [37], whereas the Mn^{2+} ions can be incorporated into the ZnS lattice in a large proportion.

Fig. 2a and b show the TEM, HRTEM, FFT and SAED images of the ZnS:Cu^{2+}(1%) NWs. The TEM image (Fig. 2a) shows that these NWs are smooth and uniform over their entire lengths and the diameter is in the range of 8–17 nm. The FFT image (see inset of Fig. 2b) further proves that the NWs grow along the (002) axis, which is in agreement with the results of XRD. The well-crystallized wurtzite form can be verified based on the discrete bright spots in the SAED image (see inset of Fig. 2b), indicating that the Cu^{2+} ions do not degrade the crystallinity of ZnS NWs. Moreover, the expanding lattice can be observed in the yellow rectangle area in Fig. 2b. Consequently, the Cu^{2+} ions have been incorporated into the ZnS lattice. The TEM and HRTEM images of the ZnS:Cu^{2+}(1%)Mn^{2+}(5%) NWs exhibit good crystallization and well oriented in Fig. 2c and d. Moreover, the degree of the lattice expand is different from the yellow rectangle regions in Fig. 2d, indicating that both the Cu^{2+} and Mn^{2+} ions have substituted for the Zn^{2+} sites simultaneously. In order to confirm the existence of the Mn^{2+} and Cu^{2+} ions, the EDAX spectra of the $Zn_{0.99}Cu_{0.01}S$:Mn^{2+} (z%) (z = 1, 5, 10) NWs were recorded. In Figs. 2e–g, it is obvious that the sample contains the Zn, S, Mn and Cu elements and the content of the Mn element is increased as the concentration of the Mn^{2+} ions increased. There is no other element in the spectra, confirming the purity of the samples.

Fig. 3a exhibits the XPS survey spectra of the ZnS:Cu^{2+}(1%) and ZnS:Cu^{2+}(1%)Mn^{2+}(5%) NWs. The presence of the carbon and oxygen are due to the carbon tape used for the measurement and the adsorbed gaseous molecules such as O_2, CO_2, and H_2O, respectively [38]. Fig. 3b and c show the high resolution XPS spectra for the S element of the ZnS:Cu^{2+}(1%) and ZnS:Cu^{2+}(1%)Mn^{2+}(5%) NWs. The peak can be decomposed into two Gaussian peaks centered at 161.30 eV and 162.99 eV, corresponding to the ZnS (blue dot line) [39] and Cu_2S (olive dot line) [40], respectively. It can

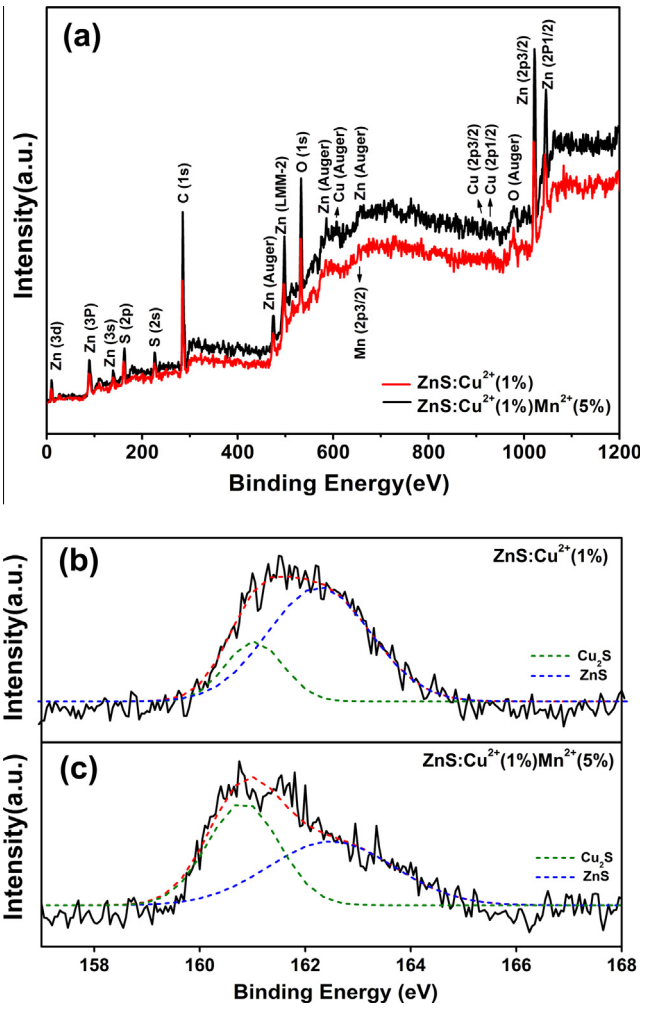

Fig. 3. (a) XPS survey spectra of the ZnS:Cu^{2+}(1%) and ZnS:Cu^{2+}(1%)Mn^{2+}(5%) NWs; (b and c) high-resolution binding energy spectra of S 2p for the ZnS:Cu^{2+}(1%) and ZnS:Cu^{2+}(1%) Mn^{2+}(5%) NWs.

be seen that the intensity of the peak coming from the Cu_2S (olive dot line) in ZnS:Cu^{2+}(1%)Mn^{2+}(5%) NWs (Fig. 4c) is higher than that in ZnS:Cu^{2+}(1%) NWs (Fig. 4b), which further proves that the Mn^{2+} ions play a key role in promoting the transition from the Cu^{2+} ions to the Cu^{+} ions. Moreover, the Cu^{+} ions have been proved the stable state and the S^{2-} ions can reduce the Cu^{2+} ions to the Cu^{+} ions in the literatures [41–43].Fig. 4a shows the absorption spectra of the ZnS:Cu^{2+} (x%) (x = 1, 2, 3, 5, 7) and $Zn_{0.99}Cu_{0.01}S$:Mn^{2+} (z%) (z = 1, 2, 5, 7, 10) NWs. It can be seen that the absorption maxima for the ZnS:Cu^{2+} NWs is 328 nm (x = 1), 330 nm (x = 2), 336 nm (x = 3), 338 nm (x = 5), 333 nm (x = 7), respectively, which is red-shift as the Cu^{2+} doped ratio increased. Since that the position of the absorption peak can reflect the band gap of the NWs. Based on the following relation:

$$\alpha = A(h\nu - E_g)^n/h\nu \quad (1)$$

where A is a constant and n is 1/2 for the direct band gap semiconductor. The band gap of the ZnS:Cu^{2+} NWs was found to decrease as the Cu^{2+} doped ratio increased, which may be caused by the localized energy levels of the excitation states of the Cu^{2+} ions or the increased size of the NWs. For the $Zn_{0.99}Cu_{0.01}S$:Mn^{2+} (z%) (z = 1, 2, 5, 7, 10) NWs, the absorption maxima is centered at 323 nm (z = 1), 327 nm (z = 2), 328 nm (z = 5), 328.6 nm (z = 7), 330 nm (z = 10), respectively, which can be seen in Fig. 4c. The band gap of the $Zn_{0.99}Cu_{0.01}S$:Mn^{2+} NWs is calculated to be 3.84 eV (z = 1), 3.79 eV (z = 2), 3.78 eV (z = 5), 3.77 eV (z = 7) and 3.75 eV (z = 10), respectively. After adding the Mn^{2+} ions into the $Zn_{0.99}Cu_{0.01}S$ NWs, the band gap of the $Zn_{0.99}Cu_{0.01}S$:Mn^{2+} NWs is larger than that of the $Zn_{0.99}Cu_{0.01}S$ NWs (3.78 eV) until the concentration of the Mn^{2+} ions increases to 5%. Further increasing the content of the Mn^{2+} ions would decrease the band gap of the $Zn_{0.99}Cu_{0.01}S$:Mn^{2+} NWs. So, the doping effect can modify the highest valence state and the lowest conduction state, thereby modulate the band gap [44]. Fig. 4b shows the PL spectra of the ZnS:Cu^{2+} NWs. Four emission peaks can be observed in the blue,[1] green and orange regions. The blue region peaks centered at 418 and 447 nm are attributed to the transition from the conduction band edge of ZnS to the surface states S and S vacancy [45]. The green emission peak centered at 540 nm is corresponding to the recombination from the shallow donor level (sulfur vacancy) to the t^2 level of Cu^{2+} [46,47]. The orange emission centered at 588 nm is rarely reported. Only Datta et al. [48] have observed this orange emission for the Cu^{2+} doped ZnS nanorods. So its origin is still not clear and needs further study. With the concentration of the Cu^{2+} ions increasing, the position of the green emission peak shifts from 540 to 544 nm, which may be due to the slight change of the size of the NWs [33]. Moreover, the PL intensity of the ZnS:Cu^{2+} NWs is decreased with the Cu^{2+} doped ratio increased and higher doping concentration results in a stronger quenching. Since that some defect centers would formed as the Cu^{2+} doped ratio increased, which can inhibit more electrons to be excited and lead to the enhancement of the nonradiative recombination process. Hence, we selected the $Zn_{0.99}Cu_{0.01}S$ NWs with the strongest PL intensity to synthesize the $Zn_{0.99}Cu_{0.01}S$:Mn^{2+} NWs. The room temperature PL spectra of the $Zn_{0.99}Cu_{0.01}S$:Mn^{2+} (z%) (z = 1, 2, 7) NWs are shown in Fig. 4d. It can be seen that the intensity of the $Zn_{0.99}Cu_{0.01}S$:Mn^{2+} NWs is about four times lower than that of the ZnS:Cu^{2+} NWs, indicating that incorporating the Mn^{2+} ions into the $Zn_{0.99}Cu_{0.01}S$ NWs would bring more defect states during the growth process. For the $Zn_{0.98}Cu_{0.01}Mn_{0.01}S$ NWs, the yellow–orange emission peak centered at 577 nm coming from the Mn^{2+} $^4T_1$–$6A_1$ transition can be observed [49], indicating that the Mn^{2+} ions have been incorporated into the $Zn_{0.99}Cu_{0.01}S$ NWs. The position of the two peaks in the blue region have no change compared with the ZnS:Cu^{2+} NWs, indicating that the energy levels of the S surface states and S vacancy relative to the valence band nearly keep constant in our samples. It is worth to note that another emission peak centered at 402 nm coming from the interstitial S can be observed for the $Zn_{0.99}Cu_{0.01}S$:Mn^{2+} NWs [50]. So, the Cu^{2+} related green emission peak shifts to 501 nm after incorporating the Mn^{2+} ions into the $Zn_{0.99}Cu_{0.01}S$ NWs, which is corresponding to the recombination of the electron in the interstitial S and the hole in Cu t^2 state [51]. With the Mn^{2+} doped ratio increasing, the relative intensity ratio of the green emission to the yellow–orange emission decreases, illustrating that there are more energy transferred from the Cu^{2+} ions to the Mn^{2+} ions. Consequently, the color-tunable emission can be obtained by adjusting the concentrations of the Mn^{2+} and Cu^{2+} ions in ZnS NWs.

Fig. 5 shows the magnetic hysteresis loops of the ZnS:Cu^{2+}(1%)-Mn^{2+}(z%) (z = 1, 5, 10) NWs. Since that we did not observe the ferromagnetism property either for the ZnS:Mn^{2+} or ZnS:Cu^{2+} NWs at room temperature. Consequently, the hybridization interaction between the Mn and Cu elements should be the fundamental reason for the origin of the ferromagnetism. Because Cu ($3d^{10}4s^1$) is a kind of non-magnetic element, the 3d orbitals are fully filled and hence do not contribute to the ferromagnetism. Moreover, its secondary phase such as CuS (Cu^{2+} $3d^9$) displays antiferromagnetism, Cu_2S (Cu^{+} $3d^{10}$) shows no magnetism due to the fully filled 3d orbitals

[1] For interpretation of color in Fig. 4, the reader is referred to the web version of this article.

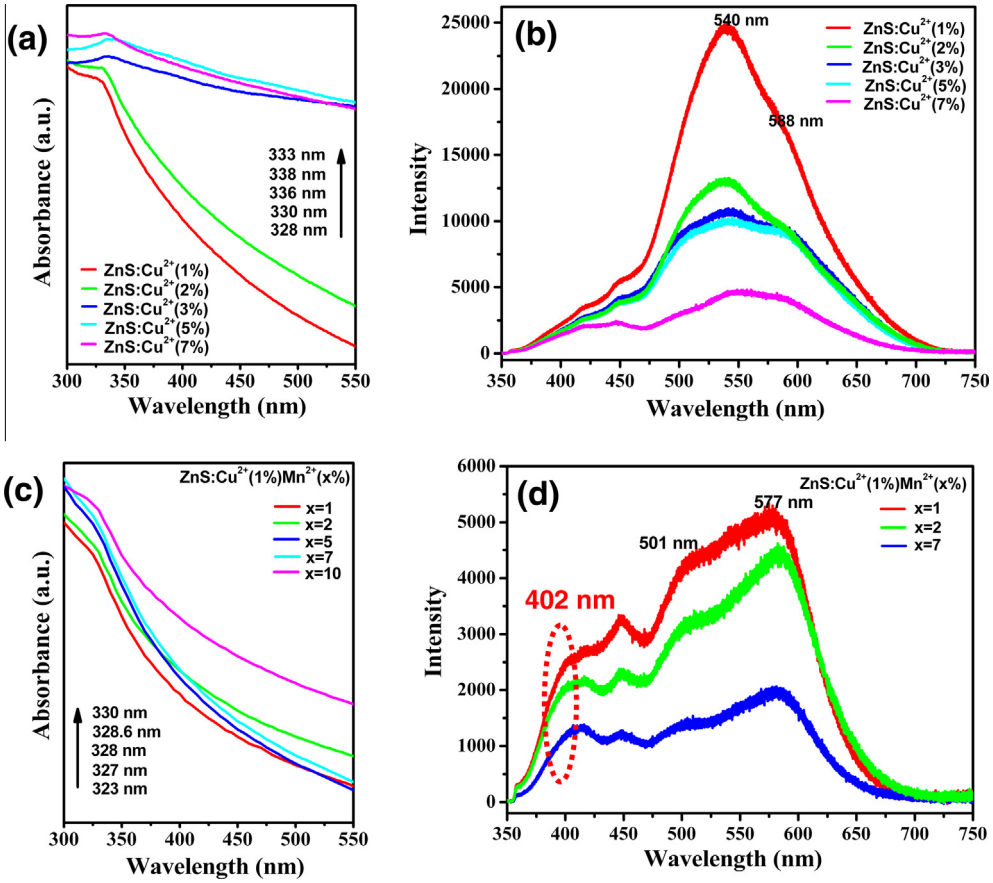

Fig. 4. (a and c) UV–vis absorption spectra of the ZnS:Cu^{2+} (x%) (x = 1, 2, 3, 5, 7) and $Zn_{0.99}Cu_{0.01}S$:Mn^{2+} (z%) (z = 1, 2, 5, 7, 10) NWs; (b and d) PL spectra of the ZnS:Cu^{2+} (x%) (x = 1, 2, 3, 5, 7) and $Zn_{0.99}Cu_{0.01}S$:Mn^{2+} (z%) (z = 1, 2, 7) NWs.

[52]. In addition, Mn itself is anti-ferromagnetic, so the extrinsic ferromagnetism cannot be induced even if the Mn clustering occurs [24]. To date, there are limited literatures about the magnetism of the Mn/Cu co-doped ZnS NWs for comparison. Chen [32] have studied the magnetic properties of the Mn/Fe co-doped ZnS NWs using the first-principle calculation. They found that the defects in the doped system favored the ferromagnetic property. During the experiment, no Mn or Cu related secondary phase or defect can be detected by the XRD analysis. Hence it may be concluded that the observed ferromagnetism is not due to the presence of any secondary phases. Since that all the spin majority states are occupied for the Mn^{2+} and Cu^{2+} ions, spin-minority states are either empty (for Mn^{2+} ions) or partially occupied (for Cu^{2+} ions). Based on the Anderson's super exchange [53], due to the hybridization between the Mn^{2+}/Cu^{2+} ion's d shell and the near neighbor S^{2-} ion's p shell, these spin-minority states become partly occupied. Consequently, the spin-majority states of the S^{2-} ions become more occupied than the spin minority states. So, the magnetic moments of the S^{2-} ions are parallel to that of the Mn^{2+}/Cu^{2+} ions [54]. It can be seen that the ferromagnetism is stronger as the Mn^{2+} doped ratio increased. Since that the results of XRD and XPS show that the Mn^{2+} ions can promote the transition from the Cu^{2+} ions to the Cu^{+} ions in the ZnS:Cu^{2+}(1%)Mn^{2+}(z%) (z = 5, 10) NWs. So the local concentration of the hole at the anion would increase, making the exchange interaction between the S^{2-} ions and the transition metal ions increased, which lead to the enhancement of the ferromagnetism [33]. In so doing, we have created multifunctional one-dimensional NWs with exciting magnetic–optical behavior at room temperature, indicating its important applications for functional nanoscale devices.

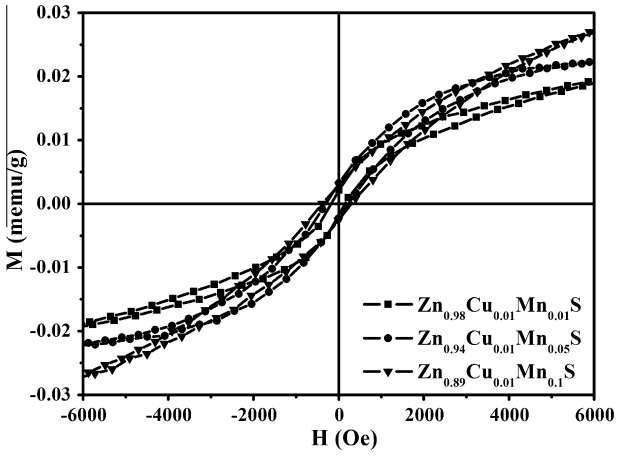

Fig. 5. Magnetic hysteresis loops of the ZnS:Cu^{2+}(1%)Mn^{2+}(1%), ZnS:Cu^{2+}(1%)-Mn^{2+}(5%) and ZnS:Cu^{2+}(1%)Mn^{2+}(10%) NWs.

4. Conclusions

In summary, we successfully synthesized ZnS:Cu^{2+}(x%), ZnS:Mn^{2+}(1%)Cu^{2+}(y%) and ZnS:Cu^{2+}(1%)Mn^{2+}(z%) NWs. Both of the Mn^{2+} and Cu^{2+} ions substituted for the Zn^{2+} sites in the host

ZnS, and the maximum doping concentration of the Cu^{2+} ions in the ZnS and ZnS:Mn^{2+}(1%) NWs, and the Mn^{2+} ions in the ZnS:Cu^{2+}(1%) NWs was 7%, 1%, 10% respectively. The result showed that the Mn^{2+} ions can promote the transition from the Cu^{2+} ions to the Cu^{+} ions. The Cu related emission peak centered at 540 nm for the ZnS:Cu^{2+} NWs and 501 nm for the ZnS:$Mn^{2+}Cu^{2+}$ NWs were observed. The Mn^{2+} $^4T_1$–$6A_1$ emission centered at 577 nm can also be observed in the ZnS:$Mn^{2+}Cu^{2+}$ NWs. As the Mn^{2+} doped ratio increased, the PL intensity was decreased and the saturation magnetization was increased.

Acknowledgments

This work was financially supported by the National Natural Science Foundation of China (Grant Nos. 61008051, 61178074, 11204104 and 11254001), the Twentieth Five-Year Program for Science and Technology of Education Department of Jilin Province (Item No. 20110169) and the Science and Technology bureau of Key Program for Ministry of Education (Item No. 20110705G).

References

[1] X.P. Song, S.W. Shi, C.B. Cao, X.S. Chen, J.B. Cui, G. He, Z.Q. Sun, J. Alloys Comp. 551 (2013) 430.
[2] F.A. La Porta, M.M. Ferrer, Y.V.B. de Santana, C.W. Raubach, V.M. Longo, J.R. Sambrano, E. Longo, J. Andrés, M.S. Li, J.A. Varela, J. Alloys Comp. 556 (2013) 153.
[3] J.D. Fan, C. Fabrega, R. Zamani, A. Shavel, F. Guell, A. Carrete, T. Andreu, A.M. Lopez, J.R. Morante, J. Arbiol, A. Cabot, J. Alloys Comp. 555 (2013) 213.
[4] M. Ragam, G. Kalaiselvan, S. Arumugam, N. Sankar, K. Ramachandran, J. Alloys Comp. 541 (2012) 222.
[5] M. Lei, X.L. Fu, P.G. Li, W.H. Tang, J. Alloys Comp. 509 (2011) 5769.
[6] M.A. Mahdi, J.J. Hassan, Z. Hassan, S.S. Ng, J. Alloys Comp. 541 (2012) 227.
[7] R. Mariappana, M. Ragavendarb, V. Ponnuswamya, J. Alloys Comp. 509 (2011) 7337.
[8] S. Kumar, C.L. Chen, C.L. Dong, Y.K. Ho, J.F. Lee, T.S. Chan, R. Thangavel, T.K. Chen, B.H. Mok, S.M. Rao, M.K. Wu, J. Alloys Comp. 554 (2013) 357.
[9] Y. Huang, W. Jie, Y. Zhou, G. Zha, J. Alloys Comp. 549 (2013) 184.
[10] W. Zhou, F. Baneyx, ACS Nano 5 (2011) 8013.
[11] R. Sakthi Sudar Saravanan, C.K. Mahadevan, J. Alloys Comp. 541 (2012) 115.
[12] L. Li, B.L. Zhang, M. Cao, Y. Sun, J.C. Jiang, P.F. Hu, Y. Shen, L.J. Wang, J. Alloys Comp. 551 (2013) 24.
[13] M. Stefan, E.J. Popovici, O. Pana, E. Indrea, J. Alloys Comp. 548 (2013) 166.
[14] S. Muthukumaran, M. Ashokkumar, Mater. Lett. 93 (2013) 223.
[15] A. Aboulaich, L. Balan, J. Ghanbaja, G. Medjahdi, C. Merlin, R. Schneider, Chem. Mater. 23 (2011) 3706.
[16] C. Corrado, Y. Jiang, F. Oba, M. Kozina, F. Bridges, J.Z. Zhang, J. Phys. Chem. A 113 (2009) 3830.
[17] X.F. Liu, N. Yang, H. Li, R.H. Yu, W. Wei, Mater. Lett. 92 (2013) 405.
[18] S. Yang, Y. Lial, N. Cheng, Y. Ling, J. Alloys Comp. 489 (2010) 689.
[19] B. Dong, L. Cao, G. Su, W. Liu, H. Qu, H. Zhai, J. Alloys Comp. 49 (2010) 363.
[20] J. Cao, J. Yang, Y. Zhang, L. Yang, Y. Wang, M. Wei, Y. Liu, M. Gao, X. Liu, Z. Xie, J. Alloys Comp. 486 (2009) 890.
[21] M. Kuppayee, G.K. Vanathi Nachiyar, V. Ramasamy, Appl. Surf. Sci. 257 (2011) 6779.
[22] S.S. Kumar, M.A. Khadar, K.G.M. Nair, J. Lumin. 131 (2011) 786.
[23] A. Datta, S. Biswas, S. Kar, S. Chaudhuri, J. Nanosci. Nanotechnol. 7 (2007) 3670.
[24] Q. Dai, C.E. Duty, M.Z. Hu, Small 6 (2010) 1577.
[25] S. Jana, B.B. Srivastava, N. Pradhan, J. Phys. Chem. Lett. 2 (2011) 1747.
[26] C.H. Liu, Z.F. Liu, J.W. Li, Y.B. Li, J.H. Han, Y. Wang, Z.C. Liu, J. Ya, Microelectron. Eng. 103 (2013) 12.
[27] D.H. Shin, J.H. Kim, Y.M. Shin, K.H. Yoon, E.A. Al-Ammar, B.T. Ahn, Progr. Photovolt.: Res. Appl. 21 (2013) 217.
[28] W.Q. Peng, G.W. Cong, S.C. Qu, Z.G. Wang, Opt. Mater. 29 (2006) 313.
[29] O. Ehlert, A. Osvet, M. Batentschuk, A. Winnacker, T. Nann, J. Phys. Chem. B 110 (2006) 23175.
[30] W. Wang, F. Huang, Y. Xia, A. Wang, J. Lumin. 128 (2008) 610.
[31] D.A. Reddy, S. Sambasivam, G. Murali, B. Poornaprakash, R.P. Vijayalakshmi, Y. Aparna, B.K. Reddy, J.L. Rao, J. Alloys Comp. 537 (2012) 208.
[32] H. Chen, J. Magn. Magn. Mater. 324 (2012) 2086.
[33] D.A. Reddy, G. Murali, B. Poornaprakash, R.P. Vijayalakshmi, B.K. Reddy, Appl. Surf. Sci. 258 (2012) 5206.
[34] J. Cao, J. Yang, L. Yang, M. Wei, B. Feng, D. Han, L. Fan, B. Wang, H. Fu, J. Appl. Phys. 112 (2012) 014316.
[35] Z.W. Quan, Z.L. Wang, P.P. Yang, J. Lin, J.Y. Fang, Inorg. Chem. 46 (2007) 1354.
[36] X. Wang, J. Xu, H. Chen, J. Phys. Chem. C. 112 (2008) 17581.
[37] L. Sun, C. Liu, C. Liao, C. Yan, J. Mater. Chem. 9 (1999) 1655.
[38] S. Biswas, S. Kar, S. Santra, Y. Jompol, M. Arif, S.I. Khondaker, J. Phys. Chem. C 113 (2009) 3617.
[39] V.G. Bhide, S. Salkalachen, A.C. Rastogi, C.N.R. Rao, M.S. Hegde, J. Phys. D: Appl. Phys. 14 (1981) 1647.
[40] A.N. Buckley, H.J. Wounterlood, R. Woods, Hydrometallurgy 22 (1989) 39.
[41] A.V. Isarov, J. Chrysochoos, Langmuir 13 (1997) 3142.
[42] C. Corrado, Y. Jiang, F. Oba, M. Kozina, F. Bridges, J.Z. Zhang, J. Phys. Chem. A 113 (2009) 3830.
[43] S. Sambasivam, B. Sathyaseelan, D.R. Reddy, B.K. Reddy, C.K. Jayasankar, Spectrochim. Acta A 71A (2009) 1503.
[44] V. Albe, C. Jouanin, D. Bertho, Phys. Rev. B 57 (1998) 8778.
[45] A.A. Bol, A. Meijerink, Phys. Rev. B 58 (1998) 1599.
[46] W. Peng, G. Cong, S. Qu, Z. Wang, Opt. Mater. 29 (2006) 313.
[47] A.K. Chawla, S. Singhal, S. Nagar, H.O. Gupta, R. Chandra, J. Appl. Phys. 108 (2010) 123519.
[48] A. Datta, S.K. Panda, S. Chaudhuri, J. Solid State Chem. 181 (2008) 2332.
[49] S. Kar, S. Biswas, J. Phys. Chem. 112 (2008) 11144.
[50] P. Hu, Y. Liu, L. Fu, L. Cao, D. Zhu, J. Phys. Chem. B 108 (2004) 936.
[51] E. Oliver, O. Andres, B. Miroslaw, W. Albrecht, N. Thomas, J. Phys. Chem. B 110 (2006) 23175.
[52] Z. Zhao, F. Geng, H. Cong, J. Bai, H. Cheng, Nanotechnology 17 (2006) 4731.
[53] P.W. Anderson, Phys. Rev. 79 (1950) 350.
[54] J. Xie, J. Magn. Magn. Mater. 322 (2010) L37.